Nonlinear rheometry of entangled polymeric rings and ring-linear blends

Daniele Parisi,[1,2] Maria Kaliva,[1,2] Salvatore Costanzo,[3] Qian Huang,[4] Pierre J. Lutz,[5] Junyoung Ahn,[6] Taihyun Chang,[6] Michael Rubinstein,[7,8,9,10] and Dimitris Vlassopoulos[1,2,a]

[1]*Institute of Electronic Structure and Laser, Foundation for Research and Technology Hellas (FORTH), Heraklion, Crete 70013, Greece*
[2]*Department of Materials Science and Technology, University of Crete, Heraklion, Crete 71003, Greece*
[3]*Department of Chemical, Materials, and Production Engineering, Federico II University, 80125 Naples, Italy*
[4]*Department of Chemical and Biochemical Engineering, Technical University of Denmark, 2800 Kgs. Lyngby, Denmark*
[5]*Institut Charles Sadron, CNRS UPR 22, University of Strasbourg, 67034 Strasbourg, France*
[6]*Division of Advanced Materials Science and Department of Chemistry, Pohang University of Science and Technology, Pohang 37673, South Korea*
[7]*Department of Mechanical Engineering and Materials Science, Duke University, Durham, North Carolina 27708*
[8]*Department of Biomedical Engineering, Duke University, Durham, North Carolina 27708*
[9]*Department of Chemistry, Duke University, Durham, North Carolina 27708*
[10]*Department of Physics, Duke University, Durham, North Carolina 27708*

Abstract

We present a comprehensive experimental rheological dataset for purified entangled ring polystyrenes and their blends with linear chains in nonlinear shear and elongation. In particular, data for the shear stress growth coefficient, steady-state shear viscosity, and first and second normal stress differences are obtained and discussed as functions of the shear rate, as well as molecular parameters (molar mass, blend composition, and decreasing molar mass of linear component in the blend). Over the extended parameter range investigated, rings do not exhibit clear transient undershoot in shear, in contrast to their linear counterparts and ring-linear blends. For the latter, the size of the undershoot and respective strain appear to increase with the shear rate. The universal scaling of the strain at overshoot and fractional overshoot (the ratio of the maximum to the steady-state shear stress growth coefficient) indicates subtle differences in the shear-rate dependence between rings and linear polymers or their blends. The shear thinning behavior of pure rings yields a slope nearly identical to predictions ($-4/7$) of a recent shear slit model and molecular dynamics simulations. Data for the second normal stress difference are reported for rings and ring-linear blends. While N_2 is negative and its absolute value stays below that of N_1, as for linear polymers, the ratio $-N_2/N_1$ is unambiguously larger for rings compared to linear polymer solutions with the same number of entanglements (almost by a factor of 2), in agreement with recent nonequilibrium molecular dynamics simulations. Furthermore, $-N_2$ exhibits slightly weaker shear rate dependence compared to N_1 at high rates, and the respective power-law exponents can be rationalized in view of the slit model (3/7) and simulations (0.6), although further work is needed to unravel the molecular original of the observed behavior. The comparison of shear and elongational stress growth coefficients for blends reflects the effect of ring-linear threading, which leads to significant viscosity enhancement in elongation. Along the same lines, the elongational stress is much larger than the first normal stress in shear, and their ratio is much larger for rings and ring-linear blends compared to linear polymers. This confirms the interlocking scenario of rings and their important role in mechanically reinforcing linear matrices. © *2021 The Society of Rheology.* https://doi.org/10.1122/8.0000186

I. INTRODUCTION

The rheology of entangled ring polymers has emerged as a topic at the forefront of scientific research. The reasons are the intriguing properties of these materials, which depart from their unlinked counterparts, and the potential applications of rings as elements for tailoring the flow properties of soft materials. Among the many manifestations of the uniqueness of nonconcatenated entangled rings, we mention their power-law stress relaxation [1,2], their weaker shear thinning of viscosity compared to their linear counterparts [2,3], their role in enhancing the viscosity of linear polymers [4–7], and their strong resistance to stretching (strain hardening at low stretch rates) [8–10]. These unusual phenomena can be explained by the loopy conformations of the rings that yield self-similar relaxation, threading by linear chains, and ring interlocking in an elongated melt, respectively. In a remarkable synergy of advanced characterization, rheometry, simulations and modeling, the field has thrived in the last decade and continues doing so, while several open questions remain. Clearly, for a deep understanding of the rheology of entangled ring polymers, there is a need to obtain more and reliable experimental evidence of the response of ring polymers in nonlinear shear and elongational flows. In particular, recent works with experimentally pure polystyrene rings

---

having about $Z = 5$ and 12 entanglements indicate that they exhibit much weaker shear thinning compared to their linear counterparts [3,11]. Furthermore, the specific viscosity enhancement of entangled linear polymers upon the addition of small fractions of rings was explained by invoking the constraint release process of the rings [4], whereas these blends were shown to exhibit significant strain hardening in uniaxial extension and an overshoot in the elongational stress growth coefficient which was associated with a transient threading-unthreading transition [8]. The above exciting results open new routes in molecular rheology and, particularly, in the direction of combining the features of rings and other macromolecular architectures to tune the viscoelastic properties of polymeric materials. The available evidence must be complemented by systematic experiments with different molar masses, the fraction of the ring component in blends, blend asymmetry (the ratio of components molar masses), and, eventually, different chemistry (and flexibility). Importantly, however, measuring the first normal stress difference (N_1), as well as the much-neglected second normal stress difference (N_2), in entangled rings is timely. Indeed, recent advances have facilitated the experimental investigations in this direction which, nevertheless, remain very challenging. However, we have shown recently that measuring all three material functions in high-temperature melts is possible by the appropriate use of a modular cone-partitioned plate (CPP) setup [12].

It should be noted that progress in simulations has been remarkable as well. The weaker shear thinning of rings compared to their linear counterpart, their nonlinear response at low elongational rates accompanied by extension rate thickening and ring-ring interlocking, and the threading-unthreading transition represent the punchline of the rich outcome so far [8,9,13–17]. Very recently, the N_1 and N_2 of moderately entangled poly(ethylene oxide) rings were investigated by means of atomistic molecular dynamics simulations, and it was found that the ratio $-N_2/N_1$ is clearly larger compared to linear polymers [16]. On the modeling part, the shear thinning of viscosity has been shown to be captured quantitatively by a new slit model that also explains many details of the conformation of the sheared rings [11]. It is based on the presence of two length scales: the thickness of the shear slit in the velocity gradient direction and, a smaller length scale, the tension blob size due to the strong stretching of rings in the flow direction. A ring is confined in the velocity gradient direction to the shear slit with thickness, ξ_s, that defines the shear blob with relaxation time on the order of the reciprocal shear rate $1/\dot{\gamma}$. The model further provides scaling predictions for N_1 and N_2 reciprocally proportional to these two length scales [11], which are discussed in the context of the experimental results in the present work.

In this work, we address the above challenges with one ambitious goal to provide a comprehensive set of reliable experimental nonlinear rheological data with purified entangled ring polymers and their blends with linear chains. The data involve the shear stress growth coefficient, steady-state viscosity and first and second normal stress differences, and comparison with respective elongational data. Importantly, in view of the significant role of the addition of small amounts of rings in altering the properties of linear matrices, as mentioned above, we focus on this range of ring-linear blend composition; one advantage is that, here, ring purification is not as crucial as in the study of the individual ring component or blends with large ring fraction (which are not addressed here). We discuss the delicate points and possible intricacies of the experiments, the role of blend composition, the behavior of N_1 and N_2, and the link to existing information from simulations, while we identify new challenges ahead.

II. MATERIALS AND METHODS

This study is based on measurements with 13 polystyrene (PS) samples, including pure components and blends. In particular, two linear polymers (L185 and L130) and three purified rings (R185, R90, and R30), covering the range from the onset of entanglements (R30) to well-entangled (R185) along with five symmetric linear/ring and three asymmetric linear/ring PS blends with a smaller molar mass of the linear component, were investigated. The samples were carefully characterized, and R185 and R90 were purified by liquid chromatography at the critical condition (LCCC); see Fig. S1 of the supplementary material (SM) [69]. The main molecular characteristics of the samples are listed in Table I. Sample coding reflects the molecular architecture, linear (*L*) and/or ring (*R*), followed by a number identifying the weight-average molar mass (M_w) of the polymer, expressed in kg/mol; the latter is often abbreviated as (k). The details of the synthesis, purification, and characterization schemes of R185 are described elsewhere [18–21]. The linear PS L90 was synthesized using potassium naphthalenide as an initiator in tetrahydrofuran (THF), while the ring R90 was obtained by coupling the bifunctional anionic PS with α,α' dibromo-*p*-xylene in the very dilute THF solution [22,23]. The same procedure was

TABLE I. Ring, linear, and ring-linear blend samples investigated and their key characteristics.

Sample code	Components	M_w (kg/mol)[a]	Notes	Z[b]
L185	PS linear 185 k	185	Linear	10.6
L130	PS linear 130 k	133	Linear	7.4
R185	PS ring 185 k	185	Ring	10.6
R90	PS ring 90 k	89.2	Ring	5.1
R30	PS ring 30 k	30	Ring	1.7
L185/R185	$\phi_R = 0.05$		Symmetric	10.6
	$\phi_R = 0.15$[b]		Linear/ring	10.6
	$\phi_R = 0.2$			10.6
	$\phi_R = 0.3$			10.6
L90/R90	$\phi_R = 0.72$[c]			5.1
L130/R185	$\phi_R = 0.05$		Asymmetric	7.4
	$\phi_R = 0.2$		Linear/ring	7.4
	$\phi_R = 0.3$			7.4

[a]Measured by light scattering, except for the molar mass of R30 which was determined based on PS standards.
[b]Based on the literature value for M_e and considering that rings and linear polymers have the same M_e. For asymmetric blends, it is averaged based on the weight fraction of the components.
[c]Used only for normal stress measurements.

followed for R30. After standard fractionation with benzene methanol [24], the R90 ring was further purified and characterized by a procedure similar to that followed for R185 [1,4,9]. Purification of as-prepared PS and characterization confirming the purity of the R90 are presented in Fig. S1 of SM [69]. Sample R30 was undergone multiple SEC runs (Fig. S2 [69], [24]), and the final product had an acceptable level of purity as judged by the combination of the final chromatogram and its linear rheology (discussed below). Blends are characterized by the weight fraction of rings, ϕ_R.

The Rouse, τ_R, the terminal (disentanglement), τ_d, and the ring terminal, τ_{Ring}, times of the pure components are reported in Table II at 160 °C. The relaxation times have been extracted from the linear viscoelastic master curves in terms of storage G′ and loss modulus G″ obtained through small amplitude oscillatory shear experiments at various temperatures. The inverse high-frequency crossover is assigned to the Rouse relaxation time of an entanglement strand, τ_e [4,8]. For polystyrene linear polymer chains τ_e is 0.002 s at 150 °C [4]. Times at various temperatures have been calculated by using the horizontal shift factor reported in Parisi *et al.* [4]. The Rouse time for linear polymer chains has been estimated as $\tau_R = \tau_e(N/N_e)^2$ [25,26], where N and N_e are the numbers of Kuhn monomers per chain and entanglement strand, respectively. N_e has been estimated as the ratio between the entanglement molar mass of PS, $M_e = 17.5$ kg/mol [27], and the respective molar mass of a polystyrene Kuhn segment, $M_0 = 0.72$ kg/mol [25]. The number of entanglements of the pure components (linear and ring polymers) and blends is denoted as Z. Values are reported in Table I. Note that the Rouse time of ring polymers has been estimated as ¼ of that of linear polymers with the same molar mass [28–30]. The terminal times are estimated from the inverse frequency at the crossover of the extrapolated terminal slopes of the dynamic moduli [4,9].

Blends were prepared by mixing specified amounts of rings and linear polymers (based on ϕ_R) in toluene in the dilute regime. Solutions were kept at room temperature for about 2 days and gently stirred at times in order to ensure complete dispersion. Subsequently, toluene was removed under vacuum over 7 days, and the resulting blends were press-molded into disks at 150 °C (well above the glass transition temperature) for 20 min under vacuum to reduce thermal oxidation. The same press-molding procedure was adopted for the pure components.

TABLE II. Characteristic relaxation times of the pure components at 160 °C.

Sample code	τ_R (s)	τ_d, τ_{Ring} (s)
L185	0.051	2.940
L130	0.025	0.500
R185	0.013	0.138
R90	0.003[a]	0.03
R30	0.000 34	0.008

[a]Estimated as $\frac{\tau_{R,L185k}}{4}\left(\frac{Z_{90k}}{Z_{185k}}\right)^2$, with $\tau_{R,L185k} = 0.051$, $Z_{90k} = 5.14$, and $Z_{185k} = 10.6$.

A. Shear rheology

Shear rheology experiments were performed on a rotational strain-controlled ARES rheometer (TA, USA) equipped with a force rebalance transducer 2KFRTN1. The temperature was controlled by means of a convection oven with an accuracy of ±0.1 °C and fed with nitrogen gas to minimize the risk of thermal degradation of the samples. As the investigated polymer melts are prone to edge fracture, a cone-partitioned plate (CPP) geometry was used for all the nonlinear shear experiments. Details about this geometry are reported elsewhere [3,12]. Here, a stainless steel 25 mm diameter cone with truncation equal to 0.051 mm and a cone angle of 0.1 rad was used. Various diameters for the inner partition of the CPP were used: 2, 3, 4, and 6 mm, as specified in the text below. Press-molded disks were loaded by using a centering tool, which ensures the proper centering of the sample in the measuring area. Linear viscoelastic master curves for L130, R90, and L130/R185 blends were obtained with stainless steel 8 mm diameter parallel plates at various temperatures in the range 120–160 °C. Master curves for L185, R185, and L185/R185 blends were taken from the literature [4]. The horizontal and vertical shift factors were taken from Parisi *et al.* [4].

The technique reported by Costanzo *et al.* [12] to extract the first N_1 and second N_2 normal stress differences was adopted. Briefly, the method consists of performing the start-up of shear rate experiments at various shear rates by using the CPP. The same experiments are performed with different inner partition diameters. This allows us to determine the apparent first normal stress difference ($N_{1,app}$) at different diameters but the same shear rates. For instance, $N_{1,app}$ corresponds to the apparent first normal stress difference measured with a CPP having an inner partition of radius R_{inner}. In the present case, we used two different inner partitions per shear rate, with radii $R_{inner,i}$ and $R_{inner,ii}$. The relations that correlate $N_{1,app,i}$, $N_{1,app,ii}$, N_1, and N_2 are [12]

$$N_{1,app,i} = \frac{2F_i}{\pi R_1^2} = N_1 + 2(N_1 + 2N_2)\ln\left(\frac{R}{R_{inner,i}}\right), \quad (1)$$

$$N_{1,app,ii} = \frac{2F_{ii}}{\pi R_2^2} = N_1 + 2(N_1 + 2N_2)\ln\left(\frac{R}{R_{inner,ii}}\right). \quad (2)$$

Here, F_i and F_{ii} are the normal forces exerted by the sample when the inner partition $R_{inner,i}$ or $R_{inner,ii}$ is used, respectively; R is the radius of the sample loaded in the measuring position, estimated as [12,31,32]

$$R = \left(\frac{3m}{2\pi\rho\theta}\right)^{1/3}, \quad (3)$$

where m is the sample mass, ρ is the sample density (0.995 g/cm³ for PS at 150 °C) [33], and θ is the cone angle expressed in radians. By using a sample mass between 8 and 23 mg, we obtain R values between 3.7 and 5.3 mm. Note that, with $R_{inner,i}$ and $R_{inner,ii}$ selected as 2 and 3 mm or 3 and 4 mm, respectively, the same sample mass was used. However, the latter is not a necessary condition to satisfy Eqs. (1) and (2) [12,32]. The two normal stress differences

N_1 and N_2 can be extracted by solving the system of Eqs. (1) and (2), where R is calculated according to Eq. (3). In order to ensure the same treatment of samples and reduce the concerns of possible fracture and sample accumulation in the gap between plate and partition, prior to applying a shear flow, a fresh disk was used for each shear rate. Finally, a note on the apparent normal stress is in order. The above approach is crucially important for extracting N_2 whose value is much smaller than that of N_1 (see discussion below). Indeed, by considering the different radii of geometries and samples used, the ratio $-N_2/N_1$ (not exceeding 0.5) and the weak shear rate dependence of the normal stress differences (see also discussion below), we estimate from Eq. (1) [or Eq. (2)] that the ratio $N_{1,app}/N_1$ varied between 1.15 and 1.75. In fact, the lowest and highest values were attained for L185 and R185, respectively (note, however, that the former is the only sample for which we used the $N_{1,app}$ value, in Figs. 15 and S21 of SM [69]). Therefore, the apparent first normal stress difference $N_{1,app}$ represents a reasonable estimation of the first normal stress difference, as will be discussed further below [12,32,34,35].

B. Extensional rheology

The extensional stress measurements were performed using a filament stretching rheometer (FSR) [36]. Prior to performing a measurement, the samples were molded into cylindrical test specimens with a fixed radius of either $R_0 = 2.7$ mm or $R_0 = 4.0$ mm. The aspect ratio $\Lambda_0 = L_0/R_0$, with L_0 being the initial length, was between 0.42 and 0.64. The smaller radius and lower aspect ratio were used due to the limited amount of the sample. The samples were press-molded following the same aforementioned procedure. All the samples were prestretched to a radius R_p ranging from 1.2 to 3 mm at 150–160 °C prior to the extensional experiments. After prestretching, the temperature was decreased to $T = 130$ °C for the extensional stress measurements. A few measurements were performed at 150 or 160 °C and shifted to 130 °C by using the shift factors reported in [4]. Nitrogen gas atmosphere was ensured during the whole test.

During the extensional measurements, the force $F(t)$ was measured by a load cell and the diameter $2R(t)$ at the midfilament plane was measured by means of a laser micrometer. At small deformations during the start-up of the elongational flow, part of the stress difference arises from the radial variation due to the shear components in the deformation field. This effect may be compensated by a correction factor as described elsewhere [37]. For large deformations, the correction vanishes and the radial variation of the stress in the symmetry plane becomes negligible [38].

The Hencky strain $\varepsilon(t)$ and the mean value of the stress difference $\langle\sigma_{zz} - \sigma_{rr}\rangle$ over the mid-filament plane are calculated from observations of $R(t)$ and $F(t)$ as

$$\varepsilon(t) = -2\ln\big(R(t)/R_p\big), \tag{4}$$

$$\langle\sigma_{zz} - \sigma_{rr}\rangle = \frac{F(t) - m_f g/2}{\pi R(t)^2} \frac{1}{1 + (R(t)/R_0)^{10/3}\exp(-\Lambda_0^3)/(3\Lambda_0^2)}, \tag{5}$$

where m_f is the weight of the filament and g is the gravitational acceleration. The Hencky strain rate is defined as $\dot{\varepsilon} = d\varepsilon/dt$. A control scheme [39] is employed in the FSR to ensure the accurate constant strain rate. The extensional stress growth coefficient is defined as $\bar{\eta}^+ = \langle\sigma_{zz} - \sigma_{rr}\rangle/\dot{\varepsilon}$.

III. RESULTS AND DISCUSSION

A. Linear viscoelastic characterization

Figure 1 depicts the linear viscoelastic (LVE) master curves [shifted G′ in panel (a) and shifted G″ panel (b)] for rings R185, R90, and R30; linear L185 and L130; and blends L185/R185, L130/R185, and L90/R90, at a reference temperature of 160 °C. This sets the necessary background for the present study: it confirms the power-law stress relaxation of the purified rings and at the same time, the quality of the samples. In fact, the lines through the (pure) ring data represent fits with the state-of-the-art fractal loopy globule (FLG) model, which predicts a power-law exponent of 3/7 [44]. Actually, for R30, which was multiply fractionated by standard SEC and corresponds to transition to the entanglement regime ($Z = 1.7$), the data are well-described by the model, but we also note that the linear precursor does not exhibit a
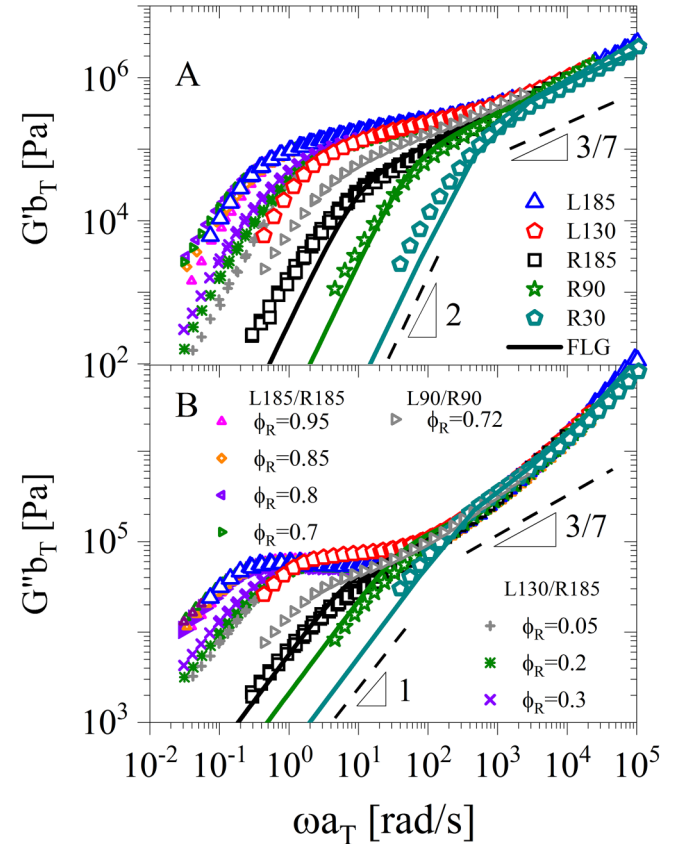

FIG. 1. Linear viscoelastic master curves of shifted storage G′ [panel (a)] and loss G″ [panel (b)] moduli as a function of shifted oscillatory frequency for pure components and blends. Details are reported in the legend. The reference temperature is 160 °C. Dashed lines with slopes 1 and 2 indicate the terminal slopes of the moduli. The solid lines represent the prediction of the fractal loopy globule (FLG) model for ring polymers [44], with a 3/7 power-law exponent for the modulus (dashed black line). Data for PS Linear 185, Ring 185, and their blends are taken from [4].

plateau; hence, our assessment of the sample's quality is based on the extracted value of the zero-rate viscosity (Fig. 2). The latter is slightly higher than expected, suggesting that this ring is not as pure as the others (which have been fractionated by LCCC) but is appropriate for use in the rheometric study discussed in Secs. III B–III D. The low-frequency deviation is attributed to remaining traces of unlinked linear and possible effects of long-living ring-ring threading [14], but overall, it remains a debatable issue that will not be discussed further. In addition, the data of Fig. 1 confirm that the blends studied here (with the fraction of the linear component being 0.7 or higher) are characterized by the presence of the rubbery plateau region. Details of their relaxation via constraint release due to linear motion are discussed in [4] and more recently in [40]. Figure 2 presents the zero-shear viscosity data for the pure components of Fig. 1 at the same reference temperature of 160 °C. The values were obtained from the complex viscosity, extracted from the lowest measured frequencies in the Newtonian regime. Data from the literature on PS of different molar masses have been added and are in excellent agreement. The slight scattering of PS ring data likely reflects a different level of purity (which remains always high) as discussed in the literature [1,18–20,24,41]. Of particular note is the striking difference in the M_w dependence of η_0 between linear and ring polymers that conforms to predictions and confirms and expands earlier data with purified rings and different chemistry [42]. There is a notable, albeit small, deviation of the data for R30, as well as for the higher molar masses. In the former case, the level of purity seems to be not as high as in the other samples, as already mentioned. In the latter case, despite the fact that even LCCC fractionation is not perfect, the ultrasmall amount of samples renders their continuous use and thermal treatment necessary, suggesting the possibility of some contamination due to unlinking of some rings. Whereas we do not know when this may happen during a measurement cycle, in an extreme case of the overused sample, we checked the linear
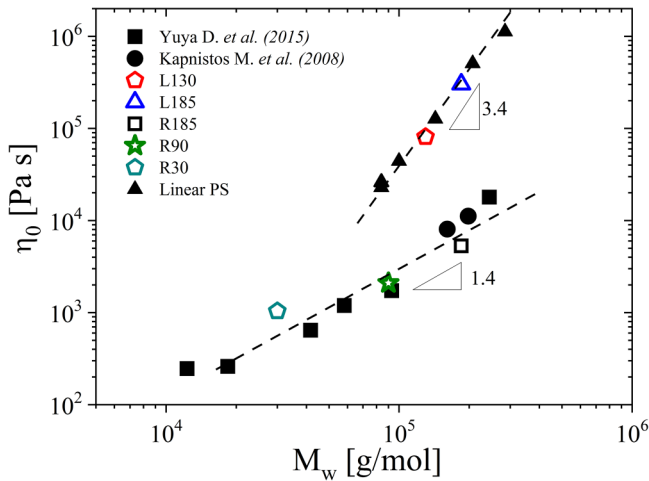

FIG. 2. Zero-shear rate viscosity η_0 as a function of the weight-average molar mass M_w for the pure components reported in Fig. 1. Additional linear PS data (solid triangles) are also reported together with high-purity ring PS from the literature [1,28]. All the data are reported at 160 °C. The dashed lines represent the scaling law expected for entangled linear polymer melts with exponent 3.4 [25] and for ring polymers with exponent 1.4 [44].

spectra and its SEC trace and found differences [43]. For the presented data, the reproducibility of the linear viscoelastic data served as an indicator of the good quality of the samples.

B. Transient shear response

In Fig. 3, we show typical results of start-up of shear experiments in the form of the shear stress growth coefficient at different imposed shear rates for the two linear polymers L185 and L130 and for two ring polymers R185 and R90 (the shear stress growth coefficient for R30 is shown in Fig. S13 of SM [69]). The range of Rouse–Weissenberg numbers ($Wi_R = \dot{\gamma}\tau_R$) explored is reported in Table III for the systems investigated in this work. The lower values of Wi_R are often within the linear regime leading to the zero-shear-rate viscosity (η_0) at long times, whereas values larger than one correspond to the stretched chain regime. Similarly, it is possible to estimate the terminal Weissenberg numbers as $Wi_d = \dot{\gamma}\tau_d$ and $Wi_{Ring} = \dot{\gamma}\tau_{Ring}$ for linear chains or blends, and for pure rings, respectively.

All other transient data are presented in the SM, Figs. S3–S13 [69]. It is encouraging that the respective LVE envelope, as deduced from the respective frequency spectra of Fig. 1 and transformed into shear stress growth coefficient by means of the Cox–Merz and Gleissle [34,45] rules, match the low-shear-rate start-up data. Furthermore, the fact that the steady state is reached for shear rates covering more than two decades is a testimony of the present experimental ability to study the nonlinear rheology with this type of setup reliably. The steady-state values of the shear stress growth coefficient decrease with increasing the shear rate (see further discussion below). However, we observe some differences in the time evolution of the shear stress growth coefficient of linear and ring polymers and, particularly, in the regime between the overshoot and steady state. The linear polymers exhibit a clear undershoot at high shear rates [Figs. 3(a) and 3(b)]. However, this is not the case for the rings of the same molar mass for which no undershoot is observed over the range of investigated shear rates [Figs. 3(c) and 3(d)]. Moreover, at the highest rates, the sample fractures before the steady-state value are attained (data not shown). This points to a clear difference in the shear-induced conformational changes in the two macromolecular architectures. Before further discussing the features of the undershoot, we confirm that based on careful experiments (see [12,46] and the present data), it is real. We also note that recent slip-link simulations show that undershoot is not linked to slip (which tends to suppress it) [47]. Recently, conformational differences between extended single DNA ring and linear polymers have been reported in the context of the coil-stretch transition [48]. Importantly, the undershoot (or the minimum in the transient response) of linear polymers has been linked to transient tumbling [34,46,49]; if undershoots occur in rings, this should happen at higher rates, which are not accessible experimentally at the moment. The conjecture of different conformation in sheared ring and linear polymers is supported by recent insightful evidence about their response in the dilute or nondilute solution from both experiments
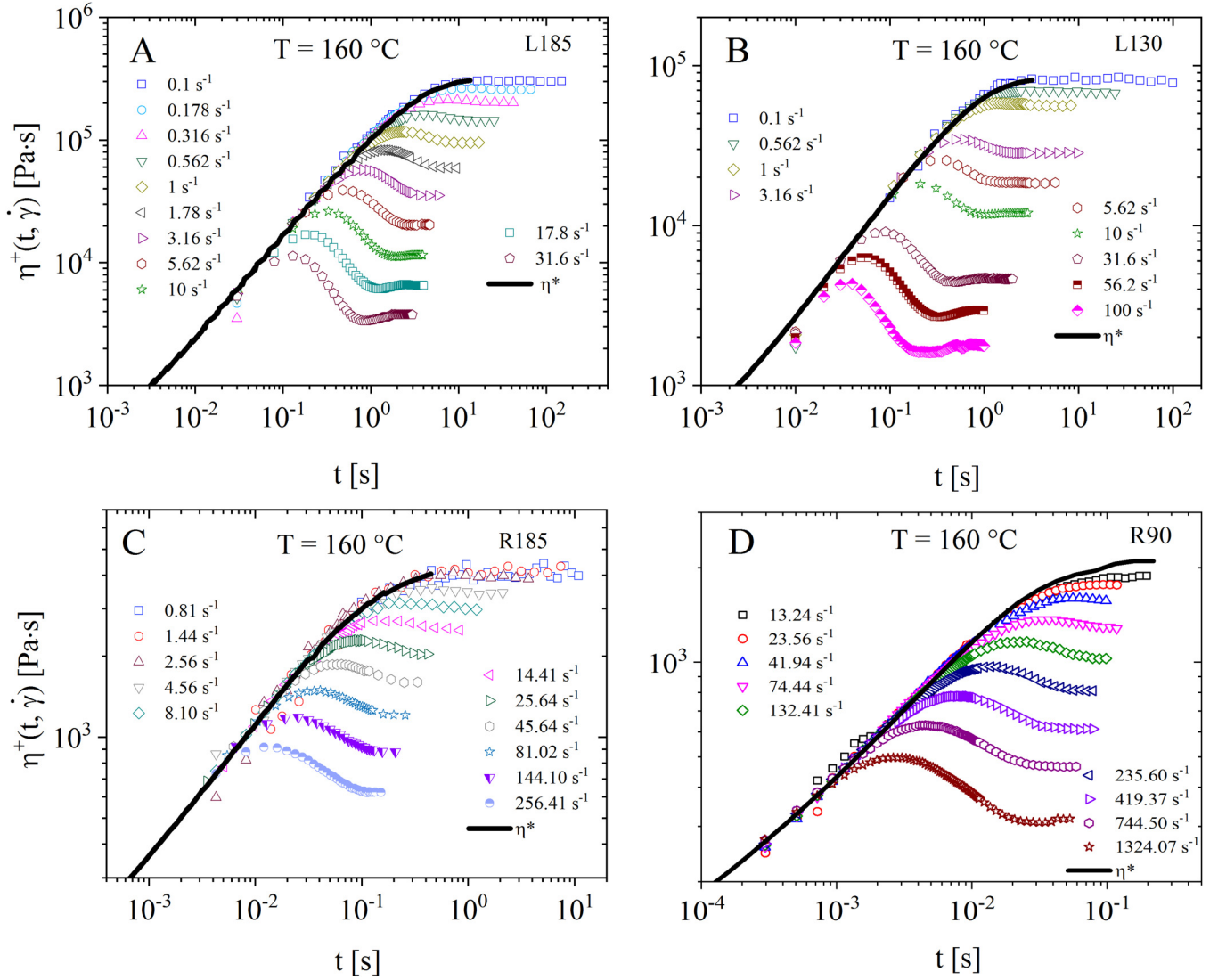
FIG. 3. Shear rate start-up in terms of the shear stress growth coefficient as a function of time at various shear rates (reported in the legend) for (a) L185, (b) L130, (c) R185, and (d) R90. Experimental data refer to the same temperature, 160 °C. The sample R90 was measured at 130 °C, and data were shifted to 160 °C by using the shift factors reported in [4]. The R30 sample is reported in Fig. S13 of SM [69]. Black solid lines report the LVE envelope, i.e., the complex viscosity (η^*) as a function of the inverse oscillatory frequency.

[10,50] and simulations [51–53], as well as simulations and modeling in the melt state [11,13–16].

Adding rings to linear matrices alters the nonlinear shear response in a subtle way. The message from Fig. 4 is that,

TABLE III. Wi_R range in start-up of steady shear experiments.

Sample code	Wi_R range
L185	0.005–1.6
L130	0.0025–2.5
R185	0.01–3.33
R90	0.04–4.0
R30	0.0027–0.35
L185/R185 $\phi_R = 0.05$	0.0016–0.29
L185/R185 $\phi_R = 0.2$	0.0016–2.0
L185/R185 $\phi_R = 0.3$	0.0005–2.0
L130/R185 $\phi_R = 0.05$	0.0008–1.4
L130/R185 $\phi_R = 0.2$	0.0008–1.4
L130/R185 $\phi_R = 0.3$	0.0008–0.8

even with a ring fraction as high as 0.3, the qualitative features of linear chains are predominant, similar to the conclusion based on linear viscoelasticity results [1,4–6,54]. For example, the undershoot in the transient response is observed at high shear rates. The undershoot data are presented in Fig. 5. The strain at the undershoot minimum, γ_{MIN}, increases with Weissenberg number (here we consider Wi_R) by a factor of 3 [or factor of 2 for sample L185, Fig. 5(a)] over the range of Wi_R between 0.2 and 3 approximately (range 0.5–2 for L185). The magnitude of the fractional undershoot, i.e., the ratio of the minimum to the steady-state shear stress growth coefficient, $\eta_{MIN}/\eta_{steady-state}$, systematic decreases (by about 10%) as Wi_R increases from 0.25 to 3 [Fig. 5(b)]. Interestingly, whereas the asymmetric blends exhibit undershoot, this is not the case for the symmetric ones; however, the latter were measured at lower rates at which the asymmetric blends do not exhibit undershoot either (Fig. 4). On the other hand, the largest Wi_R values reached for the rings are similar to (or even slightly larger than) Wi_R reached for the
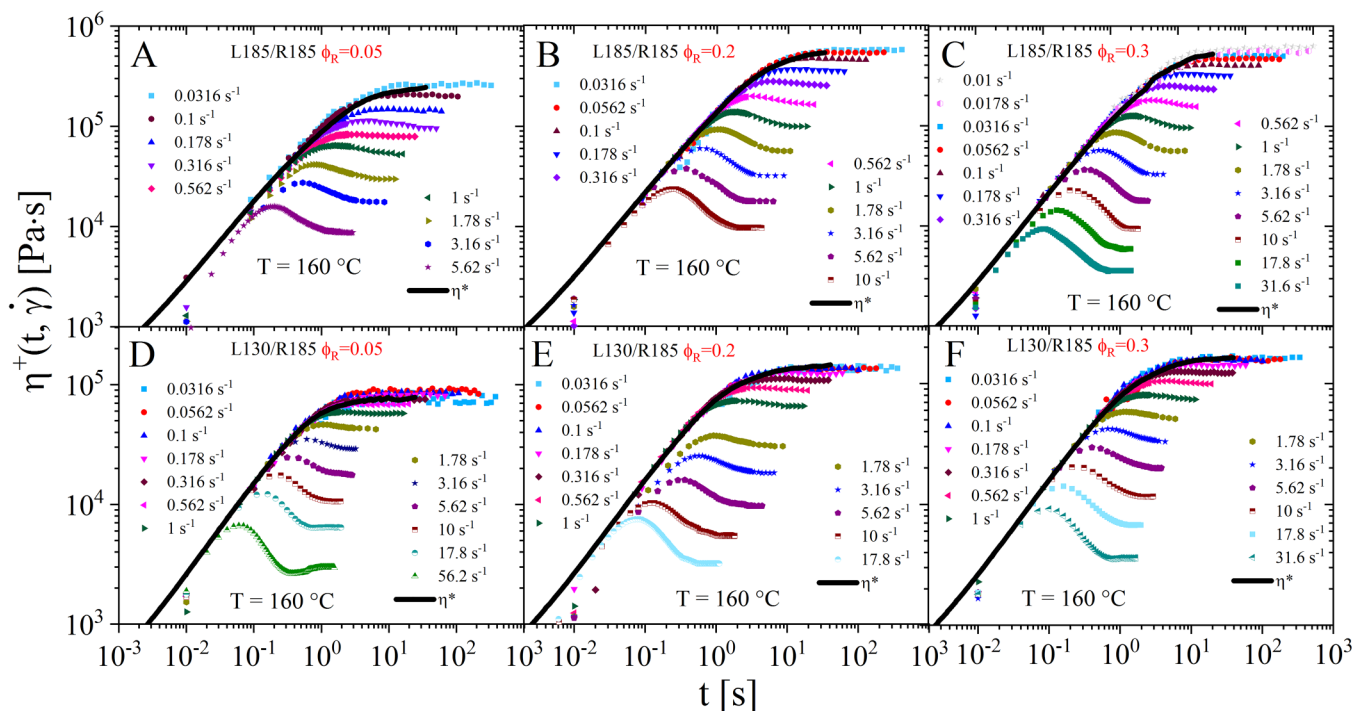
FIG. 4. Start-up of the shear rate in terms of the shear stress growth coefficient as a function of time at various shear rates (reported in the legend) for symmetric blends L185/R185 at (a) $\phi_R = 0.05$, (b) $\phi_R = 0.2$, and (c) $\phi_R = 0.3$, and for asymmetric blends L130/R185 at (d) $\phi_R = 0.05$, (e) $\phi_R = 0.2$, and (f) $\phi_R = 0.3$. Experimental data refer to the same experimental temperature, 160 °C. Black solid lines report the complex viscosity (η^*) as a function of the inverse oscillatory frequency.

symmetric blends (see Table III). Therefore, to assess the effect of decreasing molar mass of the linear component of the blend, there is a need for more investigations with experiments and simulations. Finally, it can be observed from Figs. 3 and 4 that the main features of shear thinning and the matching of the low-shear-rate data with the LVE envelope are maintained for all examined blend compositions. To better appreciate the shear thinning regime, we present in Fig. 6, the flow curves normalized by the zero-shear viscosity and the terminal time,

for both pure components [panel (a)] and blends [panel (b)]. Viscosities from oscillatory and steady shear measurements are plotted and found to validate the Cox–Merz (CM) rule with the exception of divergence of the latter data from the complex viscosity envelope for the high M_w linear chains at very high shear rates. From the experimental standpoint, the occurrence of instabilities (primarily the onset of weak wall slip and edge fracture propagating up to the gap of the CPP), cannot be avoided at large terminal Wi numbers (>30), despite the
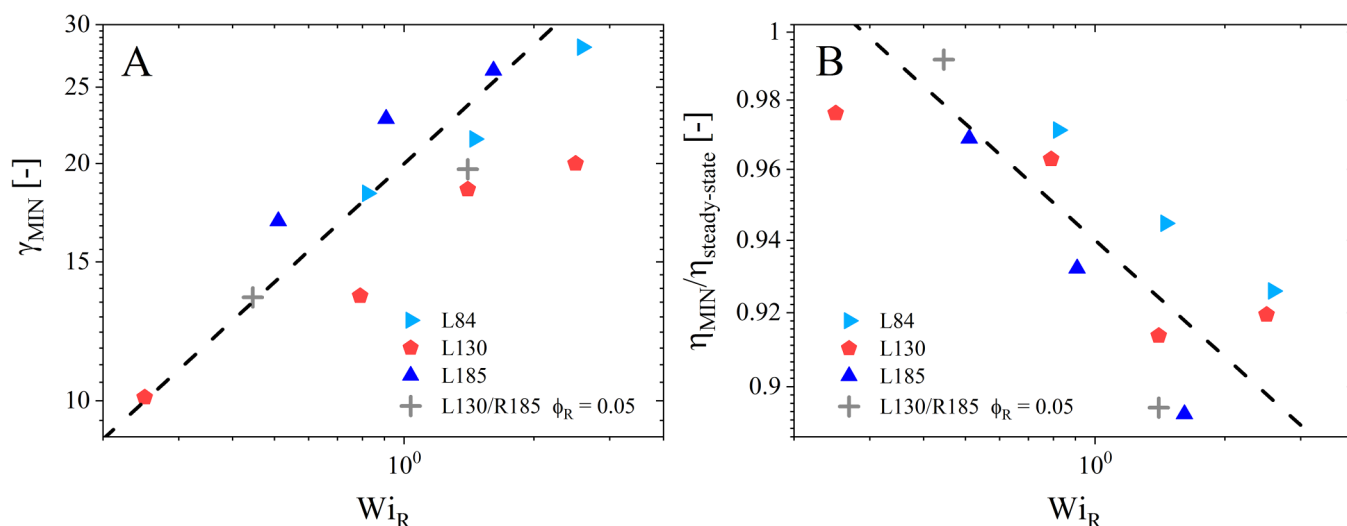

FIG. 5. Analysis of the transient undershoot: Strain at the minimum shear stress growth coefficient (a) and fractional undershoot (normalized), i.e., the ratio of minimum to steady-state shear stress growth coefficient values (b), as functions of the Rouse–Weissenberg number. Error bars are within the symbol size. Dashed lines are a guide for the eye.
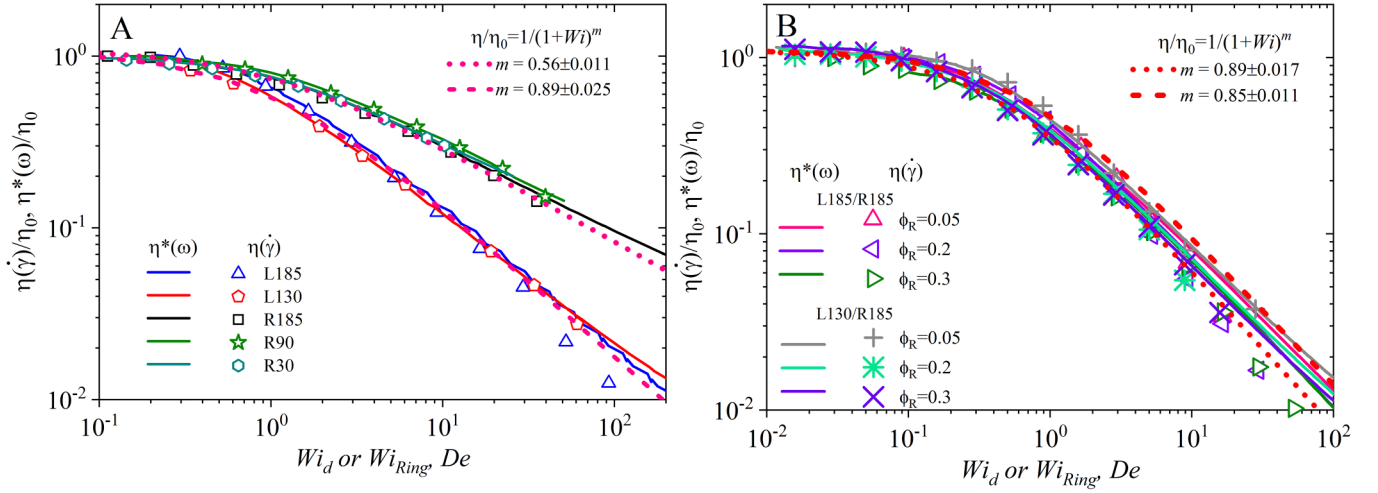
FIG. 6. Steady-shear (symbols) normalized by the zero-shear rate viscosity as a function of the shear rate normalized by the terminal relaxation time (terminal relaxation Weissenberg number Wi_d or Wi_{Ring}) and complex viscosity (lines) normalized by the zero-shear rate viscosity as a function the normalized frequency (Deborah number, De) for the pure components (a) and the blends (b). The dashed and dotted lines in panel (a) are fits with the Carreau–Yasuda model for the linear and ring polymers, respectively. The dashed and dotted lines in panel (b) are fits with the Carreau–Yasuda model for the samples with small and large fractions of rings, respectively. The shear thinning exponents are reported in the figure.

precautions taken. On the other hand, similar deviations were recently reported with simulations and attributed to reduction of the tension blob size [11]. Data are fitted with a modified Carreau–Yasuda equation [11,55,56], $\frac{\eta}{\eta_0} = 1/(1 + Wi)^m$, where m is the shear thinning exponent. The latter takes values of 0.89 for pure linear melts, between 0.85 and 0.89 for the blends, and 0.56 for the pure ring polymers, in agreement with the slit model and molecular dynamics simulations presented in [11].

A measure of the degree of deformability of polymers under shear is the fractional overshoot, i.e., the ratio of the maximum value of the shear stress growth coefficient to its steady-state values. The fractional overshoot is plotted as a

function of the Rouse–Weissenberg number Wi_R in Fig. 7, where we can clearly distinguish two groups: the pure rings collapse into one group and follow a power-law dependence $\eta_{MAX}/\eta_{steady-state}|_{rings} \sim Wi_R^{1/7}$, while all other samples (linear polymers and blends) appear to follow a distinctly different scaling behavior $\eta_{MAX}/\eta_{steady-state}|_{linear,blends} \sim Wi_R^{1/4}$ with larger fractional overshoot values. The latter dependence has been reported for many different entangled linear polymers [3,12,34,57]. We note also that theoretical predictions based on the tube model with appropriate adjustments to account for segmental orientation and stretching do capture the occurrence of overshoot [34,58,59]. A recent tube-based model, which takes into account the concept of gripping force
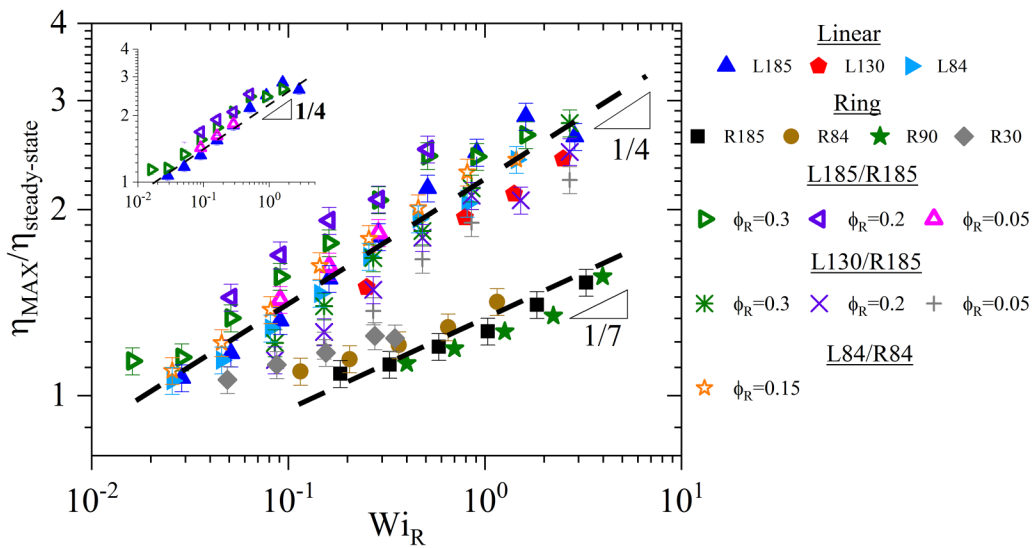

FIG. 7. The maximum overshoot in the shear stress growth coefficient normalized by its steady-state value as a function of the Rouse–Weissenberg number. The black dashed lines with slopes 1/4 and 1/7 indicate the dependence observed in the earlier analysis of entangled linear and marginally entangled ring polymers, respectively [3,34]. Data for the 84 k linear (L84) and ring (R84) polymers, as well as their blend L84/R84 are taken from the literature [3]. The inset presents the maximum shear stress growth coefficient normalized by its steady-state value for L185 and the symmetric L185/R185 blends. Symbols are listed in the legend and refer to Table I. Error bars refer to the errors in determining η_{MAX} and $\eta_{steady-state}$. When not clearly visible, the error bars are within the symbol size.

between topological constraints at shear rates exceeding the reciprocal Rouse time, also predicts the overshoot in stress growth function [60,61]. However, the extent of fractional overshoot and its experimentally observed shear rate dependence were not captured quantitatively. The experimental findings of Fig. 7 suggest that the degree of deformability is larger in the pure melts of linear polymers and linear/ring blends compared to the pure rings. Moreover, a closer look at the data indicate that ring-linear blends exhibit slightly larger fractional overshoot compared to their respective pure linear component (see the inset panel in Fig. 7). Actually, the dependence of overshoot on blend composition appears to be nonmonotonic; it is tempting to recall the nonmonotonic dependence of zero-shear viscosity on composition [4–6], but the data are too limited to draw definite conclusions. Hence, the threading of rings by linear chains should play a role in the enhanced deformation, and it also appears that the asymmetric blends (here with shorter linear component) could be slightly less effective in this respect. However, this needs further investigation.

The strain, γ_{MAX}, at the overshoot (maximum) is plotted against Wi_R in Fig. 8. A tendency of all data to follow a generic trend, albeit with some scatter, is observed. Interestingly, the high-Wi_R scaling $\gamma_{MAX} \sim Wi_R^{1/3}$ has been reported for different entangled linear polymers [34,57] and predicted by the tube-based model accounting for the gripping force [60,61]. The limited data of linear and ring-linear blends at $Wi_R < 1$ virtually collapse at the value of 2.3, the Doi–Edwards prediction for the segmental alignment in flow [26], while the rings do not seem to reach a plateau but rather exhibit a weak dependence on Wi_R (which is slightly stronger for R30). For $Wi_R > 1$, there is stretching without clearly distinguishable signatures between ring and linear polymers or their blends. Along these lines, the Hencky

strain at the maximum value of the measured elongational stress growth coefficient is shown as a function of Wi_R in the inset of Fig. 8 for pure ring and linear components and their blends, as indicated in the caption (see also relevant discussion below). Over the examined regime of $Wi_R < 1$, the elongational deformation is larger than the shear one, especially for the R185 sample exhibiting the highest fractional deformation [8,9]. The peculiar extensional response of R185 is reported elsewhere [9].

C. Steady-state normal stresses

The measurements of the normal stress differences, especially N_2, are much more challenging [12,32]. In Fig. 9, we present the apparent first normal stress difference obtained as described in Sec. II A above. Note that the transient data are not taken into consideration because they are affected by axial compliance as discussed in detail in [35]. Hence, we focus on the steady-state values. Additional experimental data, as well as reliability and reproducibility tests are presented in the SM (Figs. S14–S20) [69]. The insets of Fig. 9 demonstrate the significant result that the steady-state has been reached. The cut-off in the overshoot data reported in panel (c) at $\dot{\gamma} = 56.2\,\text{s}^{-1}$ is due to the upper limit of the normal force transducer, reached during the particular experiment with a 4 mm CPP. We note that, despite the reproducibility of the data, there are non-negligible fluctuations rendering uncertainties in the result inevitable. In this context, we note that the irregular oscillations observed in the signals of Fig. 9 do not reflect material properties but rather experimental issues. Actually, we have observed the lower quality of the apparent first normal stress difference for the smaller diameter of the plate at a given shear rate. This is due to a trade-off associated with (i) the need to obtain a signal
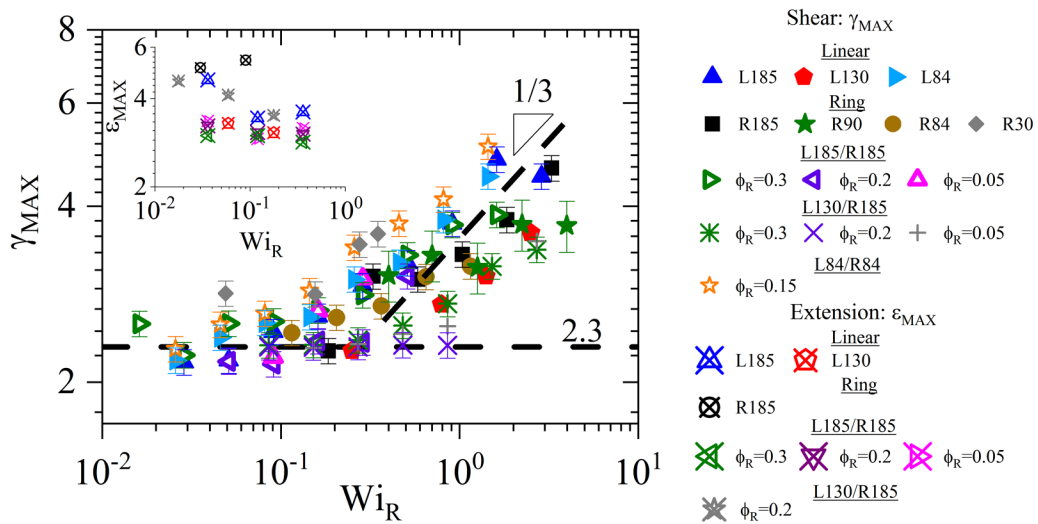

FIG. 8. Shear strain, calculated as the product of time and shear rate ($\dot{\gamma}$), at the maximum overshoot of the shear stress growth coefficient, $\dot{\gamma}$ as a function of the Rouse–Weissenberg number Wi_R for pure components and blends. Symbols are reported in the legend and refer to Table I. The horizontal dashed line at $\gamma_{MAX} = 2.3$ represents the Doi–Edwards prediction for monodisperse linear polymers [26], whereas the dashed line with slope 1/3 indicates the dependence predicted by the analysis of entangled linear and marginally entangled ring polymers, respectively [3,34,60]. The inset displays the Hencky strain at the maximum elongational stress growth coefficient as a function of Wi_R (product of the Hencky strain and rate $\dot{\varepsilon}$). Data for the 84 k linear (L84) and ring (R84) polymers, as well as their blend L84/R84 are taken from the literature [3]. Error bars represent the error in determining γ_{MAX} and ε_{MAX}. When not clearly visible, the error bars are within the symbol size.
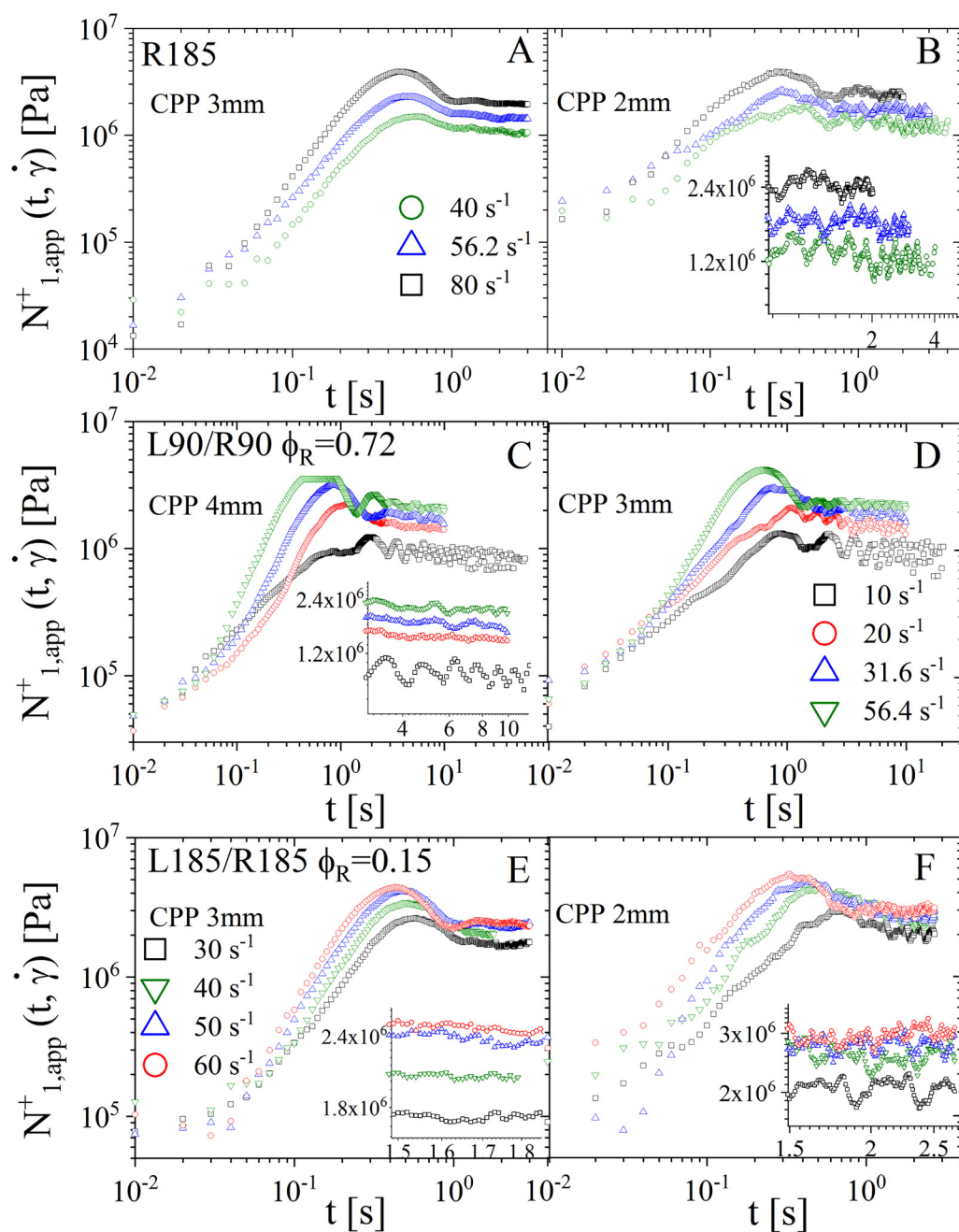
FIG. 9. Start-up of the shear rate in terms of apparent first normal stress difference, $N_{1,app}$, as a function of time at various shear rates for (i) ring R185 with (a) CPP 3 mm and (b) CPP 2 mm; (ii) blend L90/R90 at $\phi_R = 0.72$ with (c) CPP 4 mm and (d) CPP 3 mm; blend L185/R185 at $\phi_R = 0.15$ blend with (e) CPP 3 mm and (f) CPP 2 mm. Results for R185 and L90/R90 at $\phi_R = 0.72$ blend refer to 150 °C, whereas for L185/R185 at $\phi_R = 0.15$–160 °C. Insets in panels (b)–(f) show a magnification of the steady-state region. Same legends hold for panels [(a) and (b)], [(c) and (d)], and [(e) and (f)]. Data for the R30 samples are shown in Fig. S14 of SM [69].

with value below the upper limit of the axial transducer and above the resolution threshold and (ii) avoiding flow instabilities including edge fracture.

By using our method outlined in Sec. II A, we extracted the true experimental first and second normal stress differences, which are plotted as functions of the Weissenberg number in Fig. 10. The selected time for *Wi* is the terminal time assigned to the linear polymers, blends, or rings (Table II). In other words, we do not account for the slow mode of the rings, as discussed in [4,9,11]. Furthermore, we observe that $N_2 < 0$ and $|N_2| < N_1$ always, which is consistent with results from

recent nonequilibrium molecular dynamics simulations [16,62] and will be further elaborated below. Given the inevitable experimental uncertainties, despite the extra care taken during the measurements, and relatively small range of accessible rates (Table III), it is hard to draw definite conclusions about the dependence of the two normal stress differences on *Wi*. Their differences, if any, are small, as also confirmed by the recent molecular dynamics simulations with polyethylene, which for the larger investigated chains ($C_{400}H_{800}$) suggest a power-law dependence of N_1 and $|N_2|$ with an average power-law exponent of 0.6 [16,62]. Note that
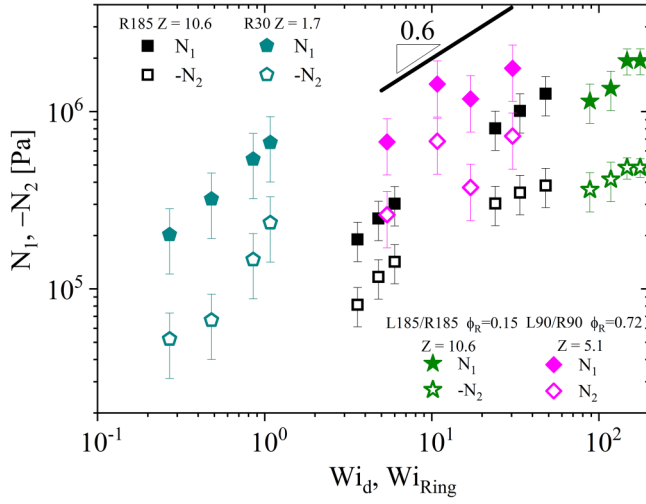
FIG. 10. Steady-state values of the first N_1 (solid symbols) and (minus) second $-N_2$ (open symbols) normal stress differences as a function of the terminal Weissenberg number (based on the terminal time for linear or blend Wi_d or the extracted ring time Wi_{Ring}) for ring R185, blend L90/R90 at $\phi_R = 0.72$ and blend L185/R185 at $\phi_R = 0.15$. The slope represents nonequilibrium molecular dynamic simulations results for ring polyethylenes [63]. Error bars are calculated by averaging out at least 20 data points in the steady state.

the reported respective exponents for linear chains, based on results of nonequilibrium molecular dynamics simulations for linear polymer melts (of chain length up to $N = 400$) are higher, 0.67 and 0.82 [63,64].

Figure 11 depicts the Wi-dependence of the ratio $-N_2/N_1$ for the measured polymers. For completeness, we add two entangled linear polystyrene solutions (in oligomers) from [12]. The value of $-N_2/N_1$ ratio is higher for pure rings and ring-linear blends, when compared to linear polymer solutions
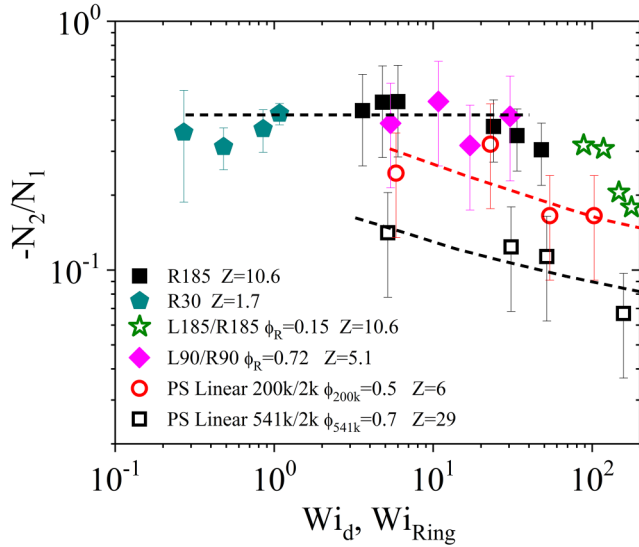

FIG. 11. Ratio of experimental steady-state (minus) second $-N_2$ and first N_1 normal stress differences as a function of the terminal Weissenberg number, Wi_d or Wi_{Ring}, for R185 (solid squares), R30 (dark cyan pentagons), L90/R90 at $\phi_R = 0.72$ (solid diamonds) and L185/R185 at $\phi_R = 0.15$ (open stars). For comparison, respective data from two PS solutions (long linear polymers diluted in oligomers) taken from the literature (open circles and squares) [12] are shown. Lines are drawn to guide the eye. Error bars are calculated by averaging at least 20 data points in the steady state.

[12]. Furthermore, a comparison based on the number of entanglements at the same Weissenberg number is more revealing. Starting from the linear polymer solutions, there seems to be a decrease in the ratio as Z increases from 6 to 29. This was attributed to the fact that samples with broader relaxation spectrum have more relaxed (faster) modes, which are not oriented and, therefore, have lower N_1 and contribute to larger $-N_2/N_1$ ratio [12]. Consequently, when the spectrum approaches a single-mode limit in the terminal regime, which is more evident for larger Z, this ratio decreases. This argument may also explain the hint of larger $-N_2/N_1$ ratio for rings.

Taking this as a basis, the limited high-Wi data of the 185 k blend with only 15 wt. % of rings and $Z = 10.6$ appear to conform to this picture. We already know that threading of rings by linear polymers strongly influences the linear and nonlinear extensional properties of the blends [4,8]. More striking are the results with the 90 k blend with $Z = 5.1$ and, importantly, the pure 185 k ring with $Z = 10.6$: the $-N_2/N_1$ ratio is clearly higher and almost constant at about 0.4 over a range of Wi covering almost 1.5 decades. This strongly suggests that ring-linear threading is very important in nonlinear shear response. The added rings are not a simple but a topological "solvent", as discussed recently [4]. Moreover, the presence of even a small fraction of rings (0.15) clearly affects the ratio $-N_2/N_1$ (see data in Fig. 11 at large values of the Weissenberg number). The experimental evidence is unfortunately limited and scattered due to the difficulty in obtaining appropriately purified ring polymers in sufficient amounts.

We now review recent results from atomistic molecular dynamics simulations with two different polymers, polyethylene [62], and poly(ethylene oxide) [16]. In the former work, the authors investigated $C_{78}H_{156}$ and $C_{400}H_{800}$ (the latter corresponding to $Z \sim 4.5$) rings and their linear counterparts and found that the ratio $-N_2/N_1$ is always larger for the rings (double) and depends on the macromolecular size. The respective ring/linear $-N_2/N_1$ ratios were 0.4/0.2 and 0.2/0.1 for $C_{78}H_{156}$ and $C_{400}H_{800}$, respectively. In the latter work, polymers with $Z \sim 0.5$, 1, and 2.5 and revealed that in all cases the ratio $-N_2/N_1$ was higher for rings, with the difference decreasing with Z and exhibiting weak shear rate dependence.

We now compare the experimental data with recent predictions of the shear slit model [11]. According to this model, the sheared ring is compressed in the velocity gradient direction into a slit of the shear blob size, giving rise to negative N_2 which is controlled by the number of monomers in a shear blob g_s (see the inset of Fig. 12). At the same time, the ring is stretched in the flow direction, with $\sigma_{xx} > \sigma_{zz}$ and $\sigma_{xx} - \sigma_{zz} = N_1 + N_2$ being controlled by the number of monomers in a tension blob g_t. This yields the following predictions:

$$N_1(\dot{\gamma}) + N_2(\dot{\gamma}) = \frac{kT\rho}{g_t(\dot{\gamma})}, \tag{6}$$

$$N_2(\dot{\gamma}) = -\frac{kT\rho}{g_s(\dot{\gamma})}, \tag{7}$$

where ρ is the number density of monomers, T is the absolute temperature, and k is Boltzmann's constant. The stronger tension in the flow direction (smaller tension blob compared to
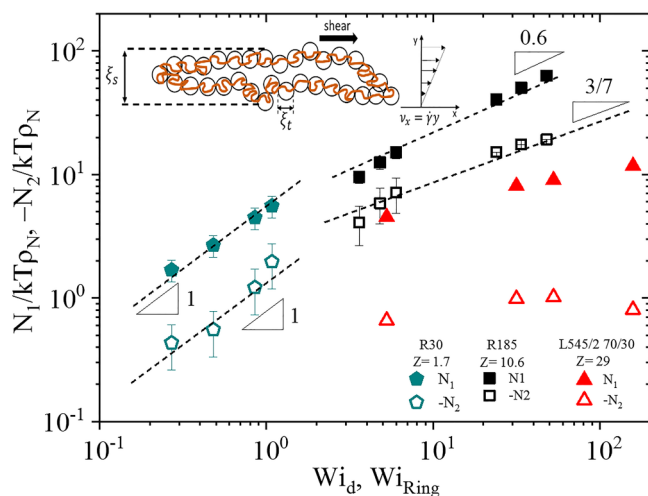
FIG. 12. Normalized steady-state values of the first (filled symbols) and second (empty symbols) normal stress differences by the thermal energy kT and the number density of chains ρ_N, i.e., number of blobs per chain, as functions of the terminal Weissenberg number, Wi_d or Wi_{Ring}. Samples R30, R185 and a linear polymer solution from [12] are reported as dark cyan pentagons, black squares and red triangles, respectively. Black dashed lines depict the 3/7 and 1 slope for the second normal stress difference data, and the 0.6 and 1 slope for the first normal stress difference (see discussion in the text), respectively.

shear blob, see also the inset of Fig. 12 and [11]) means that $N_1 > -N_2$. Therefore, Eq. (6) suggests that $N_1(\dot{\gamma}) \sim g_t(\dot{\gamma})^{-1}$. The slit model predicts [11] $g_s(\dot{\gamma}) \sim \dot{\gamma}^{-3/7}$ for $Wi_d > 1$, hence, $-N_2 \sim \dot{\gamma}^{3/7}$. On the other hand, $g_t(\dot{\gamma}) \sim \dot{\gamma}^{-x}$ with the exponent x decreasing from 12/7 to 8/7 beyond a crossover shear rate value of $Z^{7/4}/\tau_e$. This translates in respective power-law exponents for the first normal stress difference N_1 of 12/7 and 8/7.

In Fig. 12, we plot the effective number of blobs per chain as a function of the terminal Weissenberg number by scaling the experimental normal stress data with $kT\rho_N = \frac{N_A \rho_{polystyrene}}{M_w} kT$, where N_A is the Avogadro number and ρ_N is the number density of number density of chains. In general, in this representation, one may appreciate that the number of blobs per chain increases with Wi_{Ring}, or alternatively, their size decreases. We note that $-N_2$ has a slope 3/7 at higher Wi_{Ring} values, but for $Wi_{Ring} \sim 1$ (which corresponds roughly to one shear blob per chain), there seems to be a crossover toward a steeper, linear dependence. For $Wi_{Ring} \lesssim 1$, the N_1 data exhibit a similar linear dependence, which however becomes weaker at larger values of $Wi_{Ring} > 1$, departing from the predictions; the data seem to comply with the slope of about 0.6, found in recent simulations studies, as discussed above. Whereas it seems that at lower rates the dependence is slightly stronger and a crossover may take place similarly to the $-N_2$ case, this cannot be discerned given the experimental uncertainties, so we refrain from further discussing.

The discussion and proposed interpretation of the rheometric data presented and analyzed above can be summarized graphically in Fig. 13 (top), where cartoons of entangled linear polymers, entangled ring polymers, and their blends deformed in a shear field at large Weissenberg number are depicted. The message is the illustrated different deformed conformations, with stretched linear polymers forming long filaments, rings deformed in shear slits (the inset of Fig. 12), possibly with some interlocking at very large rates, and blends characterized by deformation of the threaded rings and some unthreading. Undoubtedly, a quantitative interpretation calls for further modeling and simulations, let alone
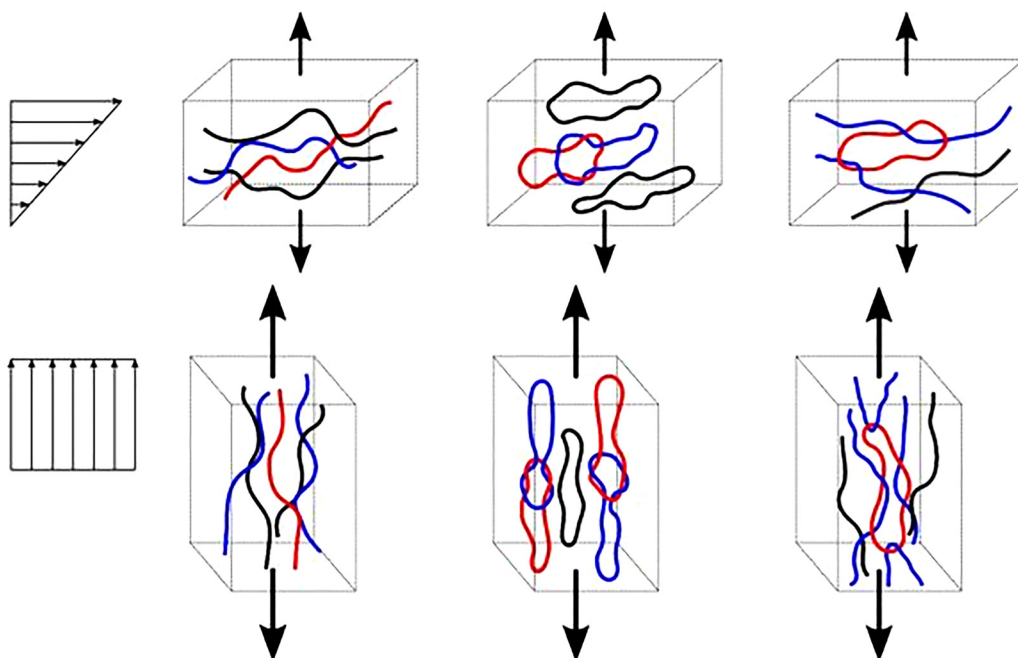

FIG. 13. Schematic illustrations of strongly deformed (at a Rouse–Weissenberg number above 1) entangled linear polymers (left), entangled ring polymers (middle), and ring-linear blends (right). Different colors (black and grey in print) are chosen for clarity of presentation (to identify individual polymers). Two deformation fields are depicted, shear (top) and uniaxial extension (bottom).

experiments. However, the key point is the consistency of the data and the possible role of the recently revealed mechanisms associated with deformed ring (e.g., threading-unthreading transition, interlocking, and weak shear thinning [3,4,8–11,17]) in the transient shear and steady normal stress responses. The above scaling model [11] represents a promising framework to understand the molecular origins of N_1 and N_2.

D. Comparison of shear and elongational response: Stress growth coefficients and stresses

It is interesting to compare the shear and extensional data (see also Fig. S22 of SM [69]). We do so in Fig. 14 for the blends and pure components, where their viscosities are plotted as a function of the Rouse–Weissenberg number, Wi_R. As a background, we note that the low-Wi_R Newtonian Trouton ratio of 3 and high-Wi_R thinning slope of linear polymers are validated, whereas rings exhibit qualitatively different behavior reflected in the low-Wi_R thickening due to ring interlocking [9,17,38], so the validity of the low-Wi_R Trouton ratio remains unclear. Note that in this representation, the elongational data of pure linear and ring components L185 and R185 do not collapse in the regime of large Wi_R, since they do so at the same elongational rates as discussed in [9]. Here, we focus on the blends for which we have sufficient experimental evidence. Based on earlier works [8,9,17], the elongation of linear and ring polymers, as well as their blends is graphically illustrated in Fig. 13 (bottom). We also recall that in the available Wi_R measured (lower for elongation), the achieved deformation is stronger in elongation compared to the shear (Fig. 8, inset). Referring to Fig. 14, given that the steady-state values of the elongational stress growth coefficient were not probed because of the sudden drop of its value after the overshoot due to the threading-unthreading transition [8], the elongational stress growth coefficient at the

maximum are reported. These values are above the respective Trouton values, as expected (since they are not the steady-state elongational viscosity values). Further, the thinning slopes of the blends follow those of the linear component, i.e., −0.82 and −0.5 for shear and elongation, respectively. From these observations, the need for further investigations of the conformational changes of threaded ring-linear blends in shear and extension by means of simulations and targeted neutron scattering experiments is evident.

We now compare in Fig. 15, the measured normal stresses in shear and elongation. Given the experimental difficulties identified above, only limited systematic data are presented. Moreover, for the same reasons, the data for the L185 sample in shear were obtained with one CPP geometry only, yielding $N_{1,app}$, and are considered acceptable for the present discussion (as also explained in the experimental Sec. II A above). This could be corroborated by the fact that the three sets of data, $N_{1,app}$ for L185 and N_1 and R185 and their blend at $\phi_R = 0.15$, nearly collapse. The first observation from Fig. 14 is that the elongational stress is much larger compared to the first normal stress difference in shear. This difference is further enhanced in pure rings compared to linear polymers (our data suggest respective values of 20 and 7 for the ratio $\langle \sigma_{zz} - \sigma_{rr} \rangle / N_1$ at the largest rates investigated). This is not surprising given that shearing motion involves both normal and shear stresses. Along these lines, it is interesting to note that the low-rate R185 ring data in elongation deviate from the established behavior of linear polymers [65,66], according to which the elongational stress is proportional to stretch rate, not to its square. This conforms to the strong thickening of rings at low elongational rates due to interlocking [17]. Unfortunately, respective low-Wi normal stress data in shear rheometric experiments could not be obtained due to instrument resolution limitations. However, the application of Laun's rule [67,68] suggests that the so-extracted elongational
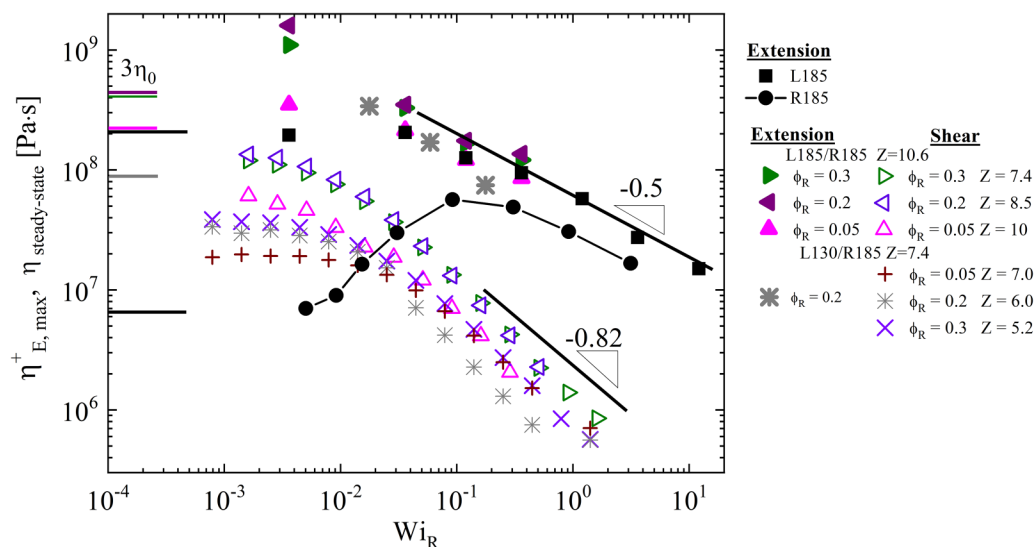

FIG. 14. Maximum elongational stress growth coefficients and steady-state shear viscosites as a function of the Rouse–Weissenberg number for ring-linear blends at 130 °C. Extensional data for L185/R185 at $\phi_R = 0.3$ are taken from [8]. Details are reported in the legend. The solid lines to the left denote the values of $3\eta_0$ for each sample (larger lines correspond to the pure L185 and R185 components). The slopes −0.5 and −0.82 describe the thinning power-law slopes in for linear polymers in uniaxial extension and shear, respectively [3,9,11,65]. Error bars calculated by averaging out at least 20 data points in the steady-state are within the symbol size.
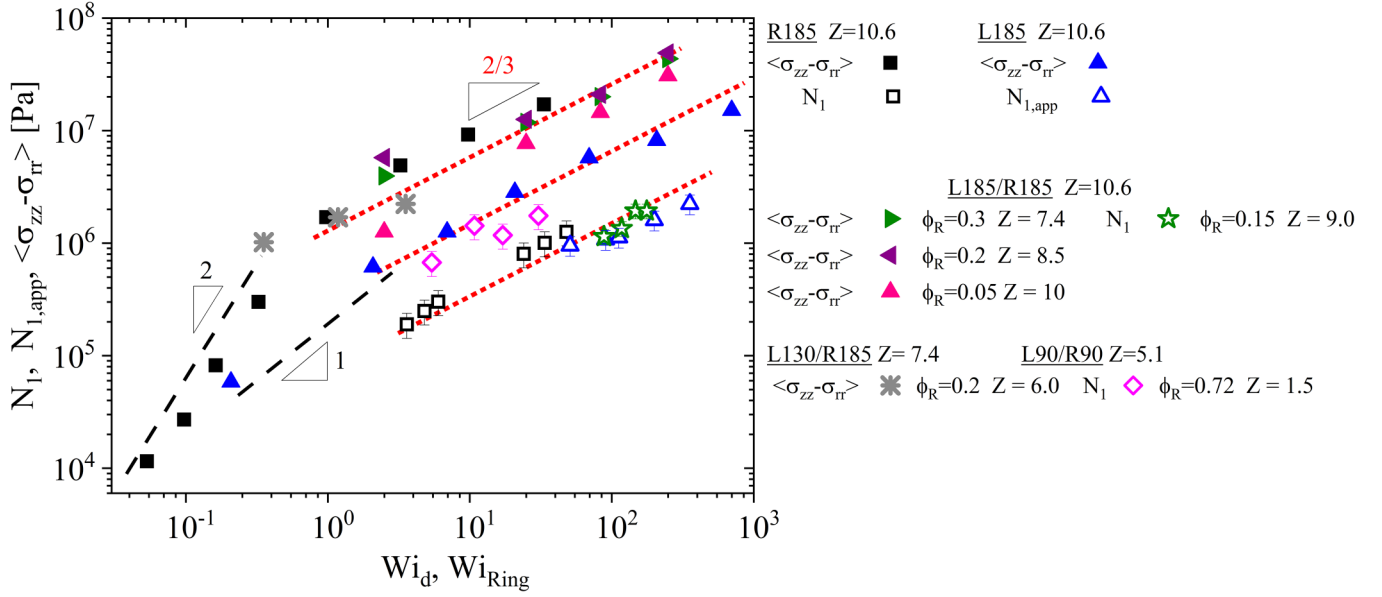
FIG. 15. Representation of the measured first normal stress difference (N_1) or its apparent value ($N_{1,app}$, see text) in shear and extensional stress ($\langle\sigma_{zz} - \sigma_{rr}\rangle$) in elongation, as a function of the Weissenberg number based on terminal time (τ_{Ring} for the rings, as noted above). Data (filled symbols for elongation, open for shear) are shown for blend L130/R185 at $\phi_R = 0.2$, linear L185, ring R185 [9], and various L185/R185 blends. The legend explains symbols and details. Lines represent limiting slopes or scaling predictions (see text). Error bars are calculated by averaging out at least 20 data points in the steady state. When not clearly visible, they are within the symbol size.

stress ring data follow the known low-shear-rate scaling with a power-law exponent of 2 (see Fig. S21 in SM [69]). Finally, turning to the blends, the same observation holds, i.e., much larger elongational stress compared to normal stress in the shear. The data with blend L185/R185 (with ring fraction not exceeding 0.3) at large rates of deformation follow the pure ring data (however, the L185 data are apparent as discussed above). This is again consistent with recent findings pointing to the role of added rings in effectively reinforcing linear matrices [4,8].

IV. CONCLUSIONS AND PERSPECTIVES

The systematic experimental study of the transient nonlinear rheology of purified entangled polystyrene rings and their blends with linear polystyrene chains has revealed several interesting new findings. The transient shear viscosity of rings barely exhibits undershoot in contrast to larger undershoot for linear chains at the same Weissenberg numbers. We expect that, if present and/or detectable, undershoot will appear at longer times at the same shear rate for rings, in comparison to their linear precursors. The shear thinning of the rings agrees with predictions of a shear slit model (with shear thinning exponent of $-4/7$). Furthermore, the stress response of symmetric and asymmetric ring-linear (with a smaller molar mass of linear component) blends with ring fraction up to 30% appears dominated by the linear component, as judged by the appearance of the undershoot, scaling of the fractional overshoot, and the strain at overshoot, as well as the shear thinning exponent. Both N_1 and $-N_2$ for rings and their blends exhibit a weak shear-rate dependence. For N_1, the data for $Wi_{Ring} > 1$ appear consistent with results from recent nonequilibrium molecular dynamics simulations

which indicate a power-law dependence with the exponent of about 0.6, whereas for $Wi_{Ring} < 1$, they seem to follow a linear dependence. Concerning $-N_2$, its rate dependence at large rates is consistent with predictions of the slit model (slope of 3/7), whereas there is a crossover to stronger dependence (slope of about 1) at lower rates corresponding to $Wi_{Ring} \sim 1$ and about one shear blob per chain. The ratio $-N_2/N_1$ for rings (of about 0.4) exceeds that of linear polymer solutions with the same number of entanglements by about a factor of 2. The larger $-N_2/N_1$ ratio result is supported by the slit model and recent nonequilibrium molecular simulations with different polymers.

Comparison of viscosities and normal stresses in shear and elongation supports the different deformation mechanisms of the ring and linear polymers (with the similar final shape of extended chains and larger tension in elongation). The ratio $\langle\sigma_{zz} - \sigma_{rr}\rangle/N_1$ is always much larger than 1 as expected and larger rings and ring-linear blends compared to linear polymers and increases with the rate of (shear or extensional) deformation. Finally, the ring response at low rates exhibits a much stronger dependence on the stretch rate compared to linear polymers, with a double power-law exponent. This evidence consistently conforms to the unique low-rate thickening of rings.

Overall, the addition of ring polymers has significant rheological consequences due to topological threading. Available data indicate that at relatively low fractions of rings, their blends with linear polymers exhibit features of both components: (i) signatures of linear in the rubbery plateau, transient shear overshoot, and undershoot (although there is a need to clarify the possible role of molar mass asymmetry, here having considered the case of the lower molar mass of the linear component), with a Wi-dependence of

fractional overshoot; and (ii) signatures of the ring in the elongational stress (following rings) and the ratio of (minus) second-to-first normal stress differences (following linear chains). At a large ring fraction, the normal stress ratio of blends seems to follow that of pure rings.

The presented data should be useful to develop a deeper understanding of the intriguing nonlinear response of ring polymers and their blends. In addition, we hope that it will trigger further studies as more experimental and simulation data are clearly needed. Importantly, in addition to simulations and further development and extension of the shear slit model (to include tumbling and model start-up in the flow), *in situ* or *ex situ* structural investigations of the sheared and elongated (e.g., [8]) rings and ring-linear blends will shed light into the mechanisms of shear deformation and possible tumbling. In this direction, polystyrenes offer the advantage for easy *ex situ* studies once quenched to room temperature at different rates (for example, this was done in [8]). This is the subject of current and future investigations.

ACKNOWLEDGMENTS

REFERENCES

[1] Kapnistos, M., M. Lang, D. Vlassopoulos, W. Pyckhout-Hintzen, D. Richter, D. Cho, T. Chang, and M. Rubinstein, "Unexpected power-law stress relaxation of entangled ring polymers," Nat. Mater. **7**, 997–1002 (2008).

[2] Halverson, J. D., W. B. Lee, G. S. Grest, A. Y. Grosberg, and K. Kremer, "Molecular dynamics simulation study of nonconcatenated ring polymers in a melt. II. Dynamics," J. Chem. Phys. **134**, 204905 (2011).

[3] Yan, Z.-C., S. Costanzo, Y. Jeong, T. Chang, and D. Vlassopoulos, "Linear and nonlinear shear rheology of a marginally entangled ring polymer," Macromolecules **49**, 1444–1453 (2016).

[4] Parisi, D., J. Ahn, T. Chang, D. Vlassopoulos, and M. Rubinstein, "Stress relaxation in symmetric ring-linear polymer blends at low ring fractions," Macromolecules **53**, 1685–1693 (2020).

[5] McKenna, G. B., and D. J. Plazek, "The viscosity of blends of linear and cyclic molecules of similar molecular mass," Polym. Commun. **27**, 304–306 (1986).

[6] Roovers, J., "Viscoelastic properties of polybutadiene rings," Macromolecules **21**, 1517–1521 (1988).

[7] Peddireddy, K. R., M. Lee, C. M. Schroeder, and R. M. Robertson-Anderson, "Viscoelastic properties of ring-linear DNA blends exhibit nonmonotonic dependence on blend composition," Phys. Rev. Res. **2**, 023213 (2020).

[8] Borger, A., W. Wang, T. C. O'Connor, T. Ge, G. S. Grest, G. V. Jensen, J. Ahn, T. Chang, O. Hassager, K. Mortensen, D. Vlassopoulos, and Q. Huang, "Threading–unthreading transition of linear-ring polymer blends in extensional flow," ACS Macro Lett. **9**, 1452–1457 (2020).

[9] Huang, Q., J. Ahn, D. Parisi, T. Chang, O. Hassager, S. Panyukov, M. Rubinstein, and D. Vlassopoulos, "Unexpected stretching of entangled ring macromolecules," Phys. Rev. Lett. **122**, 208001 (2019).

[10] Zhou, Y., K.-W. Hsiao, K. E. Regan, D. Kong, G. B. McKenna, R. M. Robertson-Anderson, and C. S. Schroeder, "Effect of molecular architecture on ring polymer dynamics in semidilute linear polymer solutions," Nat. Commun. **10**, 1–10 (2019).

[11] Parisi, D., S. Costanzo, Y. Jeong, J. Ahn, T. Chang, D. Vlassopoulos, J. D. Halverson, K. Kremer, T. Ge, M. Rubinstein, G. S. Grest, W. Srinin, and A. Y. Grosberg, "Nonlinear shear rheology of entangled polymer rings," Macromolecules **54**, 2811–2827 (2021).

[12] Costanzo, S., G. Ianniruberto, G. Marrucci, and D. Vlassopoulos, "Measuring and assessing first and second normal stress differences of polymeric fluids with a modular cone-partitioned plate geometry," Rheol. Acta **57**, 363–376 (2018).

[13] Tsolou, G., N. Stratikis, C. Baig, P. S. Stephanou, and V. G. Mavrantzas, "Melt structure and dynamics of unentangled polyethylene rings: Rouse theory, atomistic molecular dynamics simulation, and comparison with the linear analogues," Macromolecules **43**, 10692–10713 (2010).

[14] Tsalikis, D. G., V. G. Mavrantzas, and D. Vlassopoulos, "Analysis of slow modes in ring polymers: Threading of rings controls long-time relaxation," ACS Macro Lett. **5**, 755–760 (2016).

[15] Tsalikis, D. G., P. V. Alatas, L. D. Peristeras, and V. G. Mavrantzas, "Scaling laws for the conformation and viscosity of ring polymers in the crossover region around M_e from detailed molecular dynamics simulations," ACS Macro Lett. **7**, 916–920 (2018).

[16] Tsamopoulos, A. J., A. F. Katsarou, D. G. Tsalikis, and V. G. Mavrantzas, "Shear rheology of unentangled and marginally entangled ring polymer melts from large-scale nonequilibrium molecular dynamics simulations," Polymers **11**, 1194 (2019).

[17] O'Connor, T. C., T. Ge, M. Rubinstein, and G. S. Grest, "Topological linking drives anomalous thickening of ring polymers in weak extensional flows," Phys. Rev. Lett. **124**, 027801 (2020).

[18] Jeong, Y., Y. Jin, T. Chang, F. Uhlik, and J. Roovers, "Intrinsic viscosity of cyclic polystyrene," Macromolecules **50**, 7770–7776 (2017).

[19] Ziebarth, J. D., A. A. Gardiner, Y. Wang, Y. Jeong, J. Ahn, Y. Jin, and T. Chang, "Comparison of critical adsorption points of ring polymers with linear polymers," Macromolecules **49**, 8780–8788 (2016).

[20] Lee, H. C., H. Lee, W. Lee, T. Chang, and J. Roovers, "Fractionation of cyclic polystyrene from linear precursor by HPLC at the chromatographic critical condition," Macromolecules **33**, 8119–8121 (2000).

[21] Cho, D., S. Park, K. Kwon, and T. Chang, "Structural characterization of ring polystyrene by liquid chromatography at the critical condition and MALDI-TOF mass spectrometry," Macromolecules **34**, 7570–7572 (2001).

[22] Tead, S. F., E. J. Kramer, G. Hadziioannou, M. Antonietti, H. Sillescu, P. Lutz, and C. Strazielle, "Polymer topology and diffusion: A comparison of diffusion in linear and cyclic macromolecules," Macromolecules **25**, 3942–3947 (1992).

[23] McKenna, G. B., G. Hadziioannou, P. Lutz, G. Hild, C. Strazielle, C. Straupe, P. Rempp, and A. J. Kovacs, "Dilute solution characterization of cyclic polystyrene molecules and their zero-shear viscosity in the melt," Macromolecules **20**, 498–512 (1987).

[24] McKenna, G. B., B. J. Hostetter, N. Hadjichristidis, L. J. Fetters, and D. J. Plazek, "A study of the linear viscoelastic properties of cyclic polystyrenes using creep and recovery measurements," Macromolecules **22**, 1834–1852 (1989).

[25] Rubinstein, M., and R. H. Colby, *Polymer Physics* (Oxford University Press, New York, 2003).

[26] Doi, M., and S. F. Edwards, *The Theory of Polymer Dynamics* (Oxford University Press, New York, 1986).

[27] Fetters, L. J., D. J. Lohse, and R. H. Colby, Chain dimensions and entanglement spacings, in *Physical Properties of Polymers Handbook*, edited by Mark J. E. (Springer, New York, 2007), pp. 447–454.

[28] Doi, Y., K. Matsubara, Y. Ohta, T. Nakano, D. Kawaguchi, Y. Takahashi, A. Takano, and Y. Matsuhita, "Melt rheology of ring polystyrenes with ultrahigh purity," Macromolecules **48**, 3140–3147 (2015).

[29] Watanabe, H., T. Inoue, and Y. Matsumiya, "Transient conformational change of bead-spring ring chain during creep process," Macromolecules **39**, 5419–5426 (2006).

[30] Wiest, J. M., S. R. Burdette, T. W. Liu, and R. B. Bird, "Effect of ring closure on rheological behavior," J. Non-Newtonian Fluid Mech. **24**, 279–295 (1987).

[31] Meissner, J., R. W. Garbella, and J. Hostettler, "Measuring normal stress differences in polymer melt shear flow," J. Rheol. **33**, 843–864 (1989).

[32] Schweizer, T., "Measurement of the first and second normal stress differences in a polystyrene melt with a cone and partitioned plate tool," Rheol. Acta **41**, 337–344 (2002).

[33] Walsh, D., and P. Zoller, *Standard Pressure Volume Temperature Data for Polymers* (CRC, Boca Raton, FL, 1995).

[34] Costanzo, S., Q. Huang, G. Ianniruberto, G. Marrucci, O. Hassager, and D. Vlassopoulos, "Shear and extensional rheology of polystyrene melts and solutions with the same number of entanglements," Macromolecules **49**, 3925–3935 (2016).

[35] Schweizer, T., and A. Bardow, "The role of instrument compliance in normal force measurements of polymer melts," Rheol. Acta **45**, 393–402 (2006).

[36] Bach, A., H. K. Rasmussen, and O. Hassager, "Extensional viscosity for polymer melts measured in the filament stretching rheometer," J. Rheol. **47**, 429–441 (2003).

[37] Rasmussen, H. K., A. G. Bejenariu, O. Hassager, and D. Auhl, "Experimental evaluation of the pure configurational stress assumption in the flow dynamics of entangled polymer melts," J. Rheol. **54**, 1325–1336 (2010).

[38] Kolte, M. I., H. K. Rasmussen, and O. Hassager, "Transient filament stretching rheometer," Rheol. Acta **36**, 285–302 (1997).

[39] Marín, J. M. R., J. K. Huusom, N. J. Alvarez, Q. Huang, H. K. Rasmussen, A. Bach, A. L. Skov, and O. Hassager, "A control scheme for filament stretching rheometers with application to polymer melts," J. Non-Newtonian Fluid Mech. **194**, 14–22 (2013).

[40] Hou, J.-X., "Stress relaxation of entangled ring polymer chains in a linear matrix," J. Rheol. **64**, 1315–1324 (2020).

[41] Doi, Y., A. Matsumoto, T. Inoue, T. Iwamoto, A. Takano, Y. Matsushita, Y. Takahashi, and H. Watanabe, "Re-examination of terminal relaxation behavior of high-molecular-weight ring polystyrene melts," Rheol. Acta **56**, 567–581 (2017).

[42] Pasquino, R., T. C. Vasilakopoulos, Y. C. Jeong, H. Lee, S. Rogers, G. Sakellariou, J. Allgaier, A. Takano, A. R. Brás, T. Chang, S. Gooβen, W. Pyckhout-Hintzen, A. Wischnewski, N. Hadjichristidis, D. Richter, M. Rubinstein, and D. Vlassopoulos, "Viscosity of ring polymer melts," ACS Macro Lett. **2**, 874–878 (2013).

[43] Kapnistos, M., Linear and nonlinear rheology of architecturally complex polymers, Ph.D. thesis, University of California, Santa Barbara, 2006.

[44] Ge, T., S. Panyukov, and M. Rubinstein, "Self-similar conformations and dynamics in entangled melts and solutions of nonconcatenated ring polymers," Macromolecules **49**, 708–722 (2016).

[45] Cox, W. P., and E. H. Merz, "Correlation of dynamic and steady flow viscosities," J. Polym. Sci. **28**, 619–622 (1958).

[46] Stephanou, P. S., T. Schweizer, and M. Kroger, "Communication: Appearance of undershoots in start-up shear experimental findings captured by tumbling-snake dynamics," J. Chem. Phys. **146**, 161101 (2017).

[47] Masubuchi, Y., D. Vlassopoulos, G. Ianniruberto, and G. Marrucci, "Wall slip in primitive chain network simulations of shear startup of entangled polymers and its effect on the shear stress undershoot," J. Rheol. **65**, 213–223 (2021).

[48] Li, Y., K.-W. Hsiao, C. A. Brockman, D. Y. Yates, R. M. Robertson-Anderson, J. A. Kornfield, M. J. San Francisco, C. M. Schroeder, and G. B. McKenna, "When ends meet: Circular DNA stretches differently in elongational flows," Macromolecules **48**, 5997–6001 (2015).

[49] Stephanou, P. S., and M. Kröger, "Non-constant link tension coefficient in the tumbling-snake model subjected to simple shear," J. Chem. Phys. **147**, 174903 (2017).

[50] Hsiao, K.-W., C. M. Schroeder, and C. E. Sing, "Ring polymer dynamics are governed by a coupling between architecture and hydrodynamic interactions," Macromolecules **49**, 1961–1971 (2016).

[51] Liebetreu, M., M. Ripoll, and C. N. Likos, "Trefoil knot hydrodynamic delocalization on sheared ring polymers," ACS Macro Lett. **7**, 447–452 (2018).

[52] Liebetreu, M., and C. N. Likos, "Hydrodynamic inflation of ring polymers under shear," Commun. Mater. **1**, 1–11 (2020).

[53] Chen, W., J. Chen, and L. An, "Tumbling and tank-treading dynamics of individual ring polymers in shear flow," Soft Matter **9**, 4312–4318 (2013).

[54] Halverson, J. D., G. S. Grest, A. Y. Grosberg, and K. Kremer, Rheology of ring polymer melts: From linear contaminants to ring-linear blends, Phys. Rev. Lett. **138**, 038301 (2012).

[55] Carreau, P. J., "Rheological equations from molecular network theories," J. Rheol. **16**, 99–127 (1972).

[56] Yasuda, K., R. C. Armstrong, and R. E. Cohen, "Shear flow properties of concentrated solutions of linear and star branched polystyrenes," Rheol. Acta **20**, 163–178 (1981).

[57] Wang, S.-Q., *Nonlinear Polymer Rheology* (Wiley Online Library, 2018).

[58] Graham, R. S., A. E. Likhtman, T. C. McLeish, and S. T. Milner, "Microscopic theory of linear, entangled polymer chains under rapid deformation including chain stretch and convective constraint release," J. Rheol. **47**, 1171–1200 (2003).

[59] Auhl, D., J. Ramirez, A. E. Likhtman, P. Chambon, and C. Fernyhough, "Linear and nonlinear shear flow behavior of monodisperse polyisoprene melts with a large range of molecular weights," J. Rheol. **52**, 801–835 (2008).

[60] Xie, S.-J., and K. S. Schweizer, "Consequences of delayed chain retraction on the rheology and stretch dynamics of entangled polymer liquids under continuous nonlinear shear deformation," Macromolecules **51**, 4185–4200 (2018).

[61] Schweizer, K. S., and S.-J. Xie, "Physics of the stress overshoot and chain stretch dynamics of entangled polymer liquids under continuous startup nonlinear shear," ACS Macro Lett. **7**, 218–222 (2018).

[62] Yoon, J., J. Kim, and C. Baig, "Nonequilibrium molecular dynamics study of ring polymer melts under shear and elongation flows: A comparison with their linear analogs," J. Rheol. **60**, 673–685 (2016).

[63] Xu, X., J. Chen, and L. An, "Shear thinning behavior of linear polymer melts under shear flow via nonequilibrium molecular dynamics," J. Chem. Phys. **140**, 174902 (2014).

[64] Jeong, S., S. Cho, J. M. Kim, and C. Baig, "Interfacial molecular structure and dynamics of confined ring polymer melts under shear flow," Macromolecules **51**, 4670–4677 (2018).

[65] Nielsen, J. K., H. K. Rasmussen, O. Hassager, and G. H. McKinley, "Elongational viscosity of monodisperse and bidisperse polystyrene melts," J. Rheol. **50**, 453–476 (2006).

[66] Marrucci, G., and G. Ianniruberto, "Interchain pressure effect in extensional flows of entangled polymer melts," Macromolecules **37**, 3934–3942 (2004).

[67] Laun, H. M., "Prediction of elastic strains of polymer melts in shear and elongation," J. Rheol. **30**, 459–501 (1986).

[68] Sharma, V., and G. H. McKinley, "An intriguing empirical rule for computing the first normal stress difference from steady shear viscosity data for concentrated polymer solutions and melts," Rheol. Acta **51**, 487–495 (2012).

[69] See supplementary material at https://www.scitation.org/doi/suppl/10.1122/8.0000186 for sample characterization: SEC and liquid chromatography at the critical condition; nonlinear shear rheology: shear stress growth functions, steady-shear viscosities and normal forces; and nonlinear uniaxial extensional rheology.